

# Experimental Performance Evaluation of a Distributed Secondary Control Strategy for Hybrid *ac/dc*-Microgrids in the Event of Communication Loss/Delay

Enrique Espina<sup>1,2,3</sup>, Alex Navas<sup>2</sup>, Juan S. Gómez<sup>4</sup>, Roberto Cárdenas<sup>2</sup>,  
Mehrddad Kazerani<sup>3</sup>, John W. Simpson-Porco<sup>5</sup>, Doris Sáez<sup>2</sup>

<sup>1</sup>University of Santiago of Chile, Santiago, Chile. <sup>2</sup>University of Chile, Santiago, Chile.

<sup>3</sup>University of Waterloo, Waterloo, ON, Canada.

<sup>4</sup>Pontificia Universidad Católica de Chile, Santiago, Chile.

<sup>5</sup>University of Toronto, Toronto, ON, Canada. <sup>1</sup>Email: enrique.espinag@usach.cl

## Acknowledgments

This work was supported by ANID BECAS/Doctorado Nacional/2017-21171858 & 2019-21190961, in part by FONDECYT 1180879, in part by AC3E Basal Project FB0008, and in part by the Secretaría de Educación Superior, Ciencia, Tecnología e Innovación (SENESCYT) de Ecuador.

## Keywords

«Microgrid», «Smart microgrids», «Voltage Source Converter (VSC)», «Communication for Power Electronics».

## Abstract

This paper evaluates experimentally the performance of a distributed secondary control strategy applied to a hybrid *ac/dc*-microgrid in the event of common communication issues, such as communication loss and communication delays. The two scenarios are tested on a 24kW hybrid *ac/dc*-microgrid laboratory-scale prototype.

## Introduction

In recent years, the popularity of microgrids has grown due to the numerous benefits they offer, such as high reliability, flexibility and expandability [1,2]. A microgrid can be defined as a controlled small-scale power system operated in islanded or grid-connected mode to facilitate the provision of supplementary power and/or maintain a standard service [3]. The focus of the work presented in this paper is on islanded microgrids. When a microgrid is disconnected from the main grid (islanded mode), the distributed generators (*DGs*) must regulate the voltage magnitude and frequency for the *ac-DGs*, and voltage magnitude for the *dc-DGs*, to meet the corresponding grid requirements. Microgrids can be *ac* [4], *dc* [5] or hybrid *ac/dc* [6], where both *ac* and *dc* power sources and loads are integrated within the microgrid. In this work, the focus is on hybrid *ac/dc*-microgrids, as described in the next section.

As the numbers of *DGs* and agents in microgrids increase, a low-bandwidth communication network is required to improve reliability and avoid single-point failures [6, 7]. Distributed control schemes have proved to be more suitable than other approaches in maintaining high reliability and ensuring adequate operation of secondary control strategies in microgrids with a large number of *DGs* (agents) [7, 8]. A distributed control strategy (DSC) requires a distributed communication network with distributed agents performing the control actions in a cooperative fashion [9], i.e., without the need for a central controller to reach a global objective. In this paper, the performance of the distributed secondary control strategy proposed in [10] is experimentally tested and analyzed considering communication issues, such as communication loss and delays.

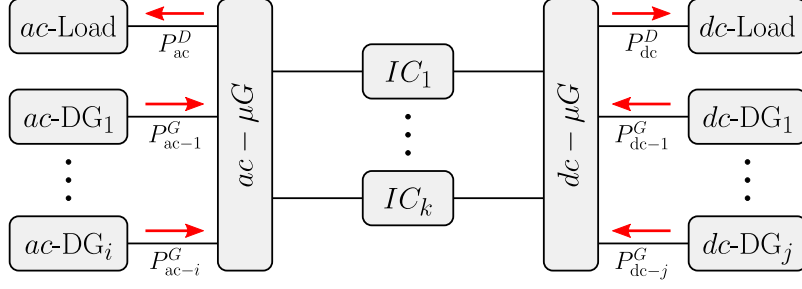


Fig. 1: A typical structure for a hybrid *ac/dc*-microgrid, with multiple *ac*-DGs, *dc*-DGs and ICs.

## Hybrid *ac/dc*-Microgrids

According to the literature [6, 11], a hybrid microgrid consists of an *ac*-microgrid and a *dc*-microgrid, connected via one or more power electronic converters capable of bidirectional power flow, called interlinking converter (*IC*), that combines the benefits of *ac*- and *dc*-microgrids. The set of devices comprising the hybrid *ac/dc*-microgrid are labelled as  $\mathbb{N}_{ac} = \{1, \dots, n\}$ ,  $\mathbb{N}_{dc} = \{n+1, \dots, n+m\}$ , and  $\mathbb{N}_{IC} = \{n+m+1, \dots, n+m+g\}$ , respectively. The general topology for the hybrid *ac/dc*-microgrid is shown in Fig. 1. The objective of the *IC* is to control bidirectional transfer of active power between the *ac*- and *dc*-sides, as well as providing reactive power on the *ac*-side to contribute to voltage regulation if it is necessary. It is claimed that with hybrid microgrids it is possible to reduce the number of power conversion stages and, thus, losses by up to 30% [12].

## Distributed Secondary Control Scheme

As described before, this paper is focused on experimentally validating the behaviour of the distributed secondary control strategy proposed in [10]. Specifically, performance of the control scheme against the most typical communication issues is analyzed.

In this strategy, the standard power-voltage ( $P/V$ ) droop controller [13] is considered as the primary control system in the *dc*-microgrid, and the standard ( $P/f$ ) and ( $Q/V$ ) droop controllers [14] are used as the primary control systems in the *ac*-microgrid. As the frequency is a global variable in the *ac*-microgrid, accurate active power-sharing is achieved in the *ac*-microgrid. On the other hand, the amplitude of the voltages is a local variable. Thus, it is not possible to achieve both accurate power-sharing and voltage restoration simultaneously for each *DG* on either side of the microgrid [8].

A global secondary control strategy for hybrid *ac/dc*-microgrids should restore the secondary variables on both sides of the microgrid, and moreover, should ensure power-sharing between all *ac*-DGs and *dc*-DGs. To achieve the latter objective, the power flowing through the *IC* must be adjusted. In the following, distributed control mechanisms proposed in [10] for achieving these goals are introduced. These control laws use peer-to-peer communication between *dc*-DGs, *ac*-DGs, and ICs.

## Controller for the *ac*-Microgrid

For the *ac*-microgrid, the secondary variables are the frequency ( $\omega_i$ ) and the amplitude ( $E_i$ ) of the voltages, while the consensus variables are the active power in p.u. ( $P_i$ ) and the reactive power in p.u. ( $Q_i$ ). Following the traditional approach, two *ac*-DSC are presented: the first one for active power-sharing and frequency restoration, and the second one for reactive power-sharing and voltage restoration.

Firstly, the *ac*-DSC for active power-sharing and frequency restoration is given by:

$$\omega_i = \omega^* + M_{ac-i} P_{ac-i} + \Psi_i \quad (1a)$$

$$\sigma_i \Psi_i = -(\omega_i - \omega^*) - \sum_{j \in \mathbb{N}_{ac}} a_{ij} (P_{ac-i} - P_{ac-j}) - \sum_{j \in \mathbb{N}_{dc}} a_{ij} (P_{ac-i} - P_{dc-j}) \quad (1b)$$

for  $i \in \mathbb{N}_{ac}$ , where  $P_{ac-j}$  is the instantaneous power generated by the  $j^{\text{th}}$  *ac*-DG  $\in \mathbb{N}_{ac}$ , and  $P_{dc-j}$  is the instantaneous power generated by the  $j^{\text{th}}$  *dc*-DG  $\in \mathbb{N}_{dc}$ .

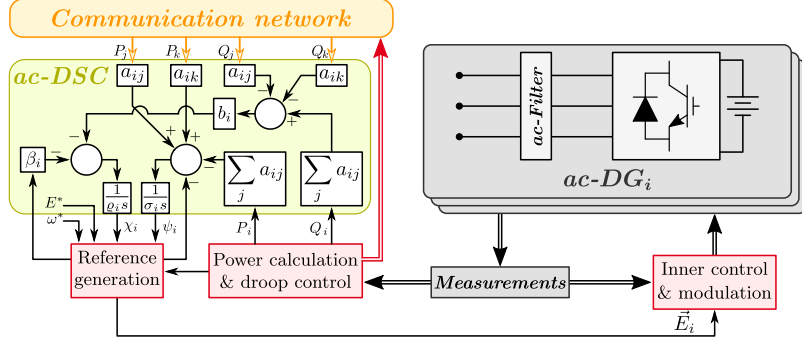


Fig. 2: Distributed secondary control for *ac*-microgrids (*ac*-DSC).

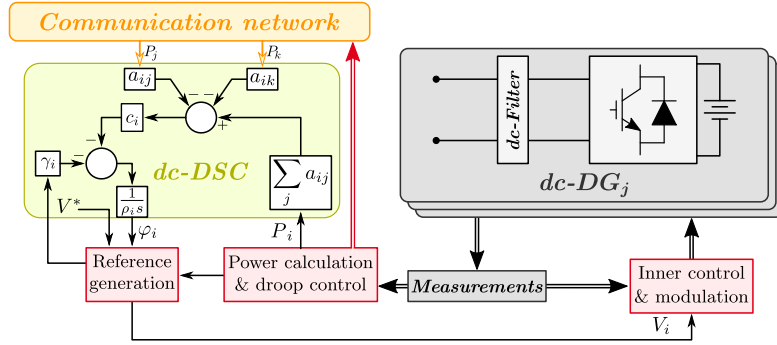


Fig. 3: Distributed secondary control for *dc*-microgrids (*dc*-DSC).

Secondly, the *ac*-DSC for reactive power-sharing and voltage restoration is given by:

$$E_i = E^* + N_{ac-i} \cdot Q_{ac-i} + \chi_i \quad (2a)$$

$$\rho_i \dot{\chi}_i = -\beta_i (E_i - E^*) - b_i \sum_{j \in \mathbb{N}_{ac}} a_{ij} (Q_i - Q_j) \quad (2b)$$

for  $i \in \mathbb{N}_{ac}$ . The gains  $M_{ac-i}, N_{ac-i} < 0$  are the primary droop gains, and  $\sigma_i, \rho_i > 0$  are time constants. The gains  $\beta_i, b_i > 0$  can be tuned to produce a compromise between voltage regulation accuracy and reactive power-sharing accuracy. A block diagram of the distributed secondary control strategy for the *ac*-DGs is shown in Fig. 2.

Although relatively similar control strategies have been studied before (see [15]), the key difference in this work is that the active power consensus of *ac*-DGs is extended to *dc*-DGs (and later, to *IC*s). This is reflected in the third term at the right hand side of (1b)], which illustrates the interaction between *ac*-DGs and *dc*-DGs, and in next sections.

### Controller for the *dc*-Microgrid

For the *dc*-microgrid, the secondary variable is the *dc*-voltage  $V_i$ , while the consensus variable is the p.u. power  $P_i$ . Then, the *dc*-DSC for power-sharing and voltage restoration is

$$V_i = V^* + M_{dc-i} \cdot P_{dc-i} + \phi_i \quad (3a)$$

$$\rho_i \dot{\phi}_i = -\gamma_i (V_i - V^*) - c_i \sum_{j \in \mathbb{N}_{dc}} a_{ij} (P_{dc-i} - P_{dc-j}) - c_i \sum_{j \in \mathbb{N}_{ac}} a_{ij} (P_{dc-i} - P_{ac-j}) \quad (3b)$$

where  $i \in \mathbb{N}_{dc}$ ,  $M_{dc-i} < 0$  is the primary control gain, and  $\rho_i > 0$  is a time constant. The gains  $\gamma_i$  and  $c_i$  can be tuned to produce a trade-off between voltage regulation accuracy and power-sharing accuracy. A block diagram of the *dc*-DSC is shown in Fig. 3.

### Controller for the *IC*

The novel consensus-based DSC strategy for the *IC*s proposed in [10] (*ic*-DSC) is slightly different than those used for *ac*-DGs and *dc*-DGs. The *IC* must regulate the power transfer between the two sides of

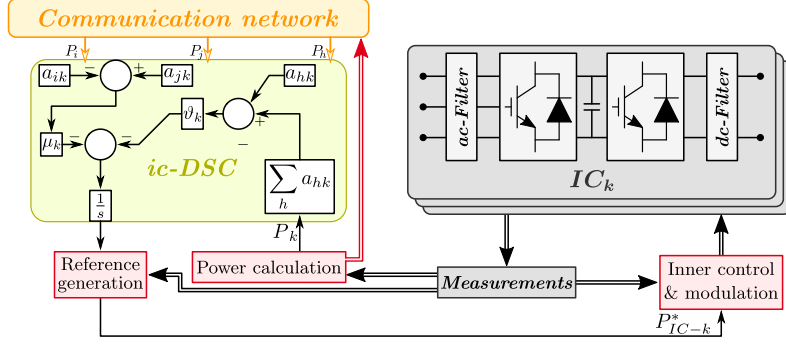


Fig. 4: Distributed secondary control for  $IC$ .

the microgrid. This has to be realized seamlessly, and without affecting the power-sharing among the  $DGs$ . To achieve this, the  $IC$  sends its own status (1: ON, 0: OFF) to the  $DGs$  in order to enable the power-consensus between the two sides of the microgrid, while the  $IC$  receives the power in p.u. being generated by the  $ac$ - $DGs$  ( $P_{ac}$ ) and by the  $dc$ - $DGs$  ( $P_{dc}$ ). Therefore, the power reference  $P_{IC-k}^*$  for the single  $k^{th}$   $IC$  ( $k = n + m + 1$ ) is updated as

$$\tau_k \dot{P}_{IC-k}^* = - \sum_{i \in \mathbb{N}_{ac}} \sum_{j \in \mathbb{N}_{dc}} a_{ik} a_{jk} (P_{ac-i} - P_{dc-j}) \quad (4)$$

where  $\tau_k > 0$  is a time constant. Note that the  $DGs$  communicating with the  $IC$  enter into the control law (4). In this work, the sign convention is that  $P_{IC-k}^* > 0$  if power flows from the  $dc$ -microgrid to the  $ac$ -microgrid. A block diagram of the  $ic$ -DSC is shown in Fig. 4.

### Communication Network

The communication network is crucial in a distributed control strategy [16]. To achieve an adequate behaviour of the controller, all the agents must have a communication link with at least one other agent [8, 17]. A typical way to describe the communication network is through an adjacency matrix  $A = [a_{ij}]$ , where the element  $a_{ij} = 1$  if  $DG_i$  is communicating with  $DG_j$ ; otherwise  $a_{ij} = 0$  [17].

## Experimental Tests

In this section, experimental test results for the hybrid  $ac/dc$ -microgrid are discussed. The experimental results validate the performance of the control strategy against communication issues.

### Experimental System

The experimental system set up for the tests is shown in Fig. 5; the topology is shown in Fig. 5a and the experimental rig is depicted in Fig. 5b. The  $ac$ -microgrid consists of three distributed generators ( $ac$ - $DGs$ ), while the  $dc$ -microgrid consists of six distributed generators ( $dc$ - $DGs$ ). Only one  $IC$  is considered. Further details are presented in [18]. The arrows represent communication links among  $DGs$ , corresponding to the adjacency matrix  $A$  shown in Fig. 5c.

Two test scenarios have been implemented: (i) Test #1 considers the disconnection and re-connection of two units (one  $ac$ - $DG$  and one  $dc$ - $DG$ ) from/to the communication network (i.e., consensus strategy), and (ii) Test #2 analyzes communication delays applied to the entire communication network. In the following, the experimental results are discussed.

#### Test #1: Communication Loss

In this test, the base case corresponds to the scenario where all units are connected to the communication network, as described in Fig. 6a. The base load condition is  $6.0kW$  for the  $ac$ -microgrid (66.6% of its nominal power) and  $9.6kW$  for the  $dc$ -microgrid (64.0% of its nominal power), as shown in Table I. For emulating the loss of communication links between  $DGs$ , units  $ac$ - $DG_1$  and  $dc$ - $DG_2$  are disconnected

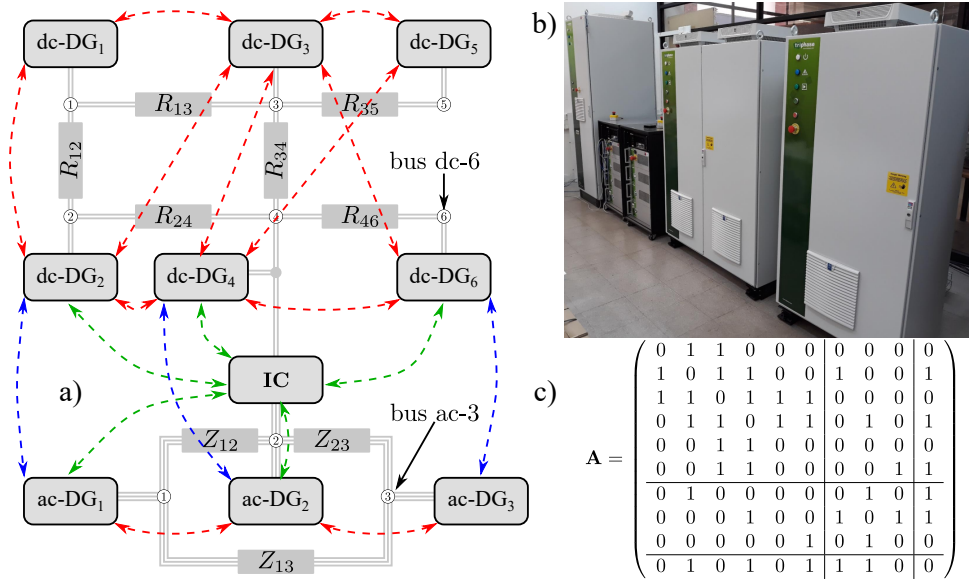


Fig. 5: Experimental hybrid *ac/dc*-microgrid. a) Topology. b) Experimental rig. c) Adjacency matrix.

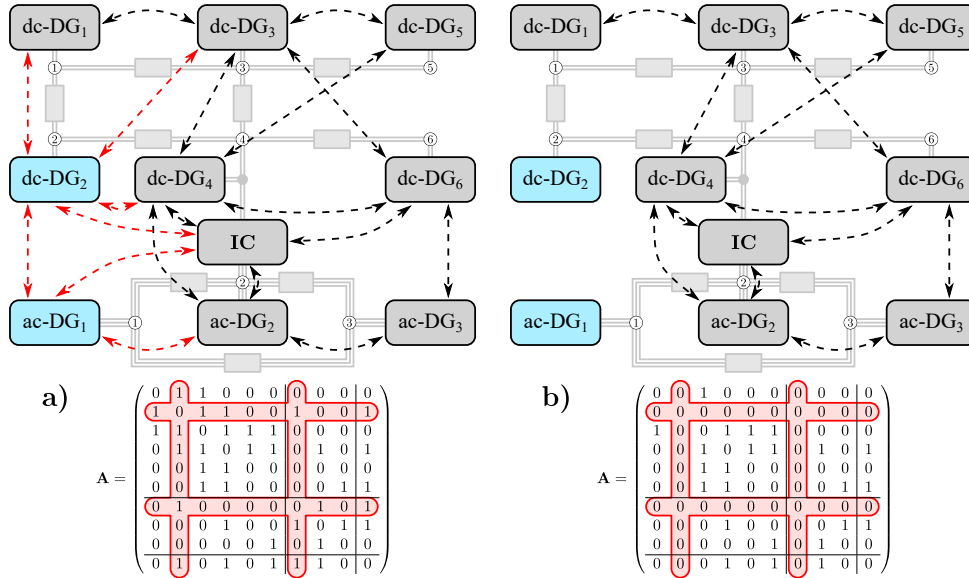


Fig. 6: Communication network for test #1. a) Normal operation. b) Communication loss operation.

from the communication network at  $t = 40s$  (see Fig. 6b), and then re-connected to the communication network at  $t = 240s$  (see Fig. 6a). The other *DGs* remain communicating for all the test.

Table I: Experimental *ac/dc*-microgrid, load conditions for test #1.

| Load  | <i>kW</i> | Load  | <i>kW</i> | Load  | <i>kVA</i>   |
|-------|-----------|-------|-----------|-------|--------------|
| $R_1$ | 2.05      | $R_4$ | 2.05      | $Z_1$ | $2.5 + j1.2$ |
| $R_2$ | 0.00      | $R_5$ | 2.05      | $Z_2$ | $2.4 + j0.0$ |
| $R_3$ | 1.37      | $R_6$ | 2.05      | $Z_3$ | $1.1 + j0.0$ |

The total power generated in this test is shown in Fig. 7a. The test begins with all the control loops activated; therefore, all the *DGs* are sharing both the active and reactive power, as shown in Fig. 7b and Fig. 7d, respectively. As the load (in p.u.) on the *ac*-side is different to that of the *dc*-side, there is a transfer of power through the *IC*, as shown in Fig. 7c.

As mentioned before, in  $t = 40s$  units  $ac-DG_1$  and  $dc-DG_2$  are disconnected from the communication

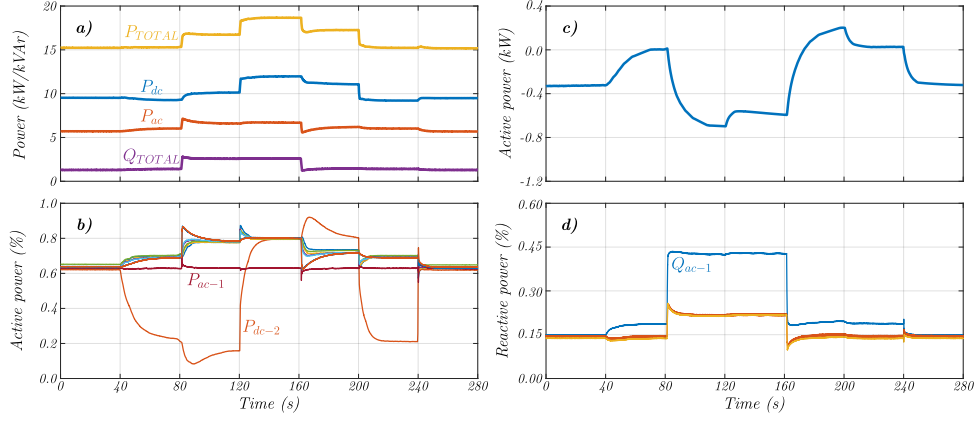


Fig. 7: Power on the hybrid *ac/dc*-microgrid for Test #1. (a) Total power (active and reactive). (b) Active power generated by *ac*-DGs ( $P_{ac-i}$ ,  $i = 1, 2, 3$ ) and *dc*-DGs ( $P_{dc-j}$ ,  $j = 1, \dots, 6$ ), in p.u. (c) Active power through the IC ( $P_{IC}$ ). (d) Reactive power generated by *ac*-DGs ( $Q_i$ ,  $i = 1, 2, 3$ ), in p.u.

network. Therefore, the disconnected units stop performing power-consensus with the other units and the distributed controllers only take care of the local variables regulation. Since the frequency is a global variable on the *ac*-side, *ac*-DG<sub>1</sub> continues supplying the same amount of power, while *dc*-DG<sub>2</sub> severely reduces the generated power (see Fig. 7b) due to now it focuses on regulating the local *dc*-voltage. Results for the secondary variables are shown in Fig. 8. The power transferred by the IC also changes when the units disconnected from the communication network stop performing power-consensus, as shown in Fig. 7c.

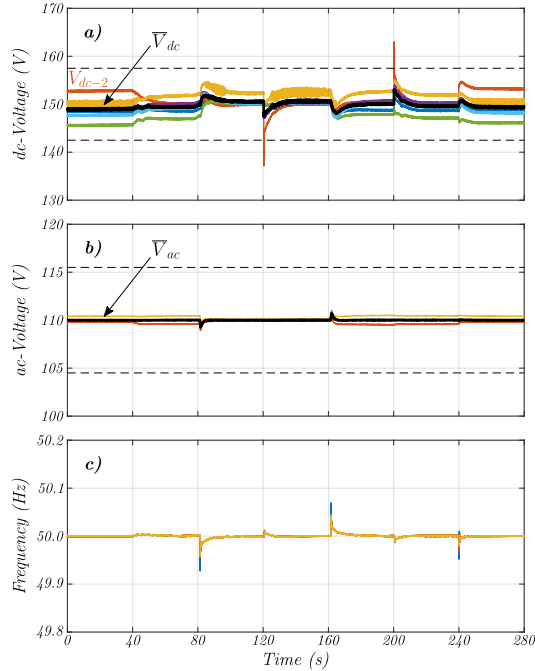


Fig. 8: Variables of the secondary control on the hybrid *ac/dc*-microgrid for Test #1. (a) Voltages on the *dc*-DGs ( $V_j$ ,  $j = 1, \dots, 6$ ). (b) Phase-to-neutral RMS voltages on the *ac*-DGs ( $V_i$ ,  $i = 1, 2, 3$ ). (c) Frequency of the voltages on the *ac*-DGs ( $f_i$ ,  $i = 1, 2, 3$ ).

Several load steps are applied on both sides of the hybrid microgrid, as follows:

- $t = 80s$  : load power in the *ac*-microgrid is increased to  $8.4kW$  (93.3%).
- $t = 120s$  : load power in the *dc*-microgrid is increased to  $11.65kW$  (77.3%).

- $t = 160s$  : load power in the  $ac$ -microgrid is decreased to  $6.0kW$  (66.6%).
- $t = 200s$  : load power in the  $dc$ -microgrid is decreased to  $9.6kW$  (64.0%).

In all cases, the units connected to the communication network continue performing the power-consensus task, while the disconnected units only regulate their local variables. The  $IC$  continues transferring power between the sub-microgrids, helping to the  $ac$ - $DGs$  to reach the power-consensus with the  $dc$ - $DGs$ , and vice versa. As soon as the units  $ac$ - $DG_1$  and  $dc$ - $DG_2$  are re-connected to the communication network, at  $t = 240s$ , they participate in the power consensus and continue performing the secondary variable regulation. Therefore, the proposed control strategy is validated against communication loss issues.

## Test #2: Communication Delays

In this test, a constant delay  $\tau_d$  is introduced in the consensus terms of the controllers for analyzing the performance of the controller against communication delays, as shown in (5)-(8). The tested cases are:

- base case ( $\tau_d = 0.0s$ ),
- small time-delay ( $\tau_d = 0.1s$ ),
- medium time-delay ( $\tau_d = 0.5s$ ), and
- large time-delay ( $\tau_d = 1.0s$ ).

$$\sigma_i \Psi_i = -(\omega_i - \omega^*) + \Psi_{ac-i} + \Psi_{dc-i} \quad (5a)$$

$$\Psi_{ac-i} = -\sum_{j \in \mathbb{N}_{ac}} a_{ij} (P_{ac-i} - P_{ac-j}(t - \tau_d)) \quad (5b)$$

$$\Psi_{dc-i} = -\sum_{j \in \mathbb{N}_{dc}} a_{ij} (P_{ac-i} - P_{dc-j}(t - \tau_d)) \quad (5c)$$

$$\rho_i \Phi_i = -\gamma_i (V_i - V^*) + \Phi_{dc-i} + \Phi_{ac-i} \quad (6a)$$

$$\Phi_{dc-i} = -c_i \sum_{j \in \mathbb{N}_{dc}} a_{ij} (P_{dc-i} - P_{dc-j}(t - \tau_d)) \quad (6b)$$

$$\Phi_{ac-i} = -c_i \sum_{j \in \mathbb{N}_{ac}} a_{ij} (P_{dc-i} - P_{ac-j}(t - \tau_d)) \quad (6c)$$

$$\tau_k \dot{P}_{IC-k}^* = -\sum_{i \in \mathbb{N}_{ac}} \sum_{j \in \mathbb{N}_{dc}} a_{ik} a_{jk} (P_{ac-i} - P_{dc-j}(t - \tau_d)) \quad (7)$$

$$\rho_i \dot{\chi}_i = -\beta_i (E_i - E^*) - b_i \sum_{j \in \mathbb{N}_{ac}} a_{ij} (Q_i - Q_j(t - \tau_d)) \quad (8)$$

The base load condition is  $5.9kW$  for the  $ac$ -microgrid (65.5% of its nominal power) and  $11.6kW$  for the  $dc$ -microgrid (77.3% of its nominal power), as shown in Table II.

Table II: Experimental  $ac/dc$ -microgrid, load conditions for test #2.

| Load  | $kW$ | Load  | $kW$ | Load  | $kVA$        |
|-------|------|-------|------|-------|--------------|
| $R_1$ | 2.05 | $R_4$ | 2.05 | $Z_1$ | $1.7 + j0.0$ |
| $R_2$ | 2.05 | $R_5$ | 2.05 | $Z_2$ | $2.4 + j0.0$ |
| $R_3$ | 1.37 | $R_6$ | 2.05 | $Z_3$ | $1.8 + j0.0$ |

At  $t = 0$ , since all the control loops are activated and the system is at steady-state, both  $ac$ - $DGs$  and  $dc$ - $DGs$  are sharing the load power for all the studied values of  $\tau_d$ , as shown in Fig. 9a-d and Fig. 11a-d for active and reactive power, respectively, and the power is transferred through the  $IC$  as shown in Fig. 9e-h. On the other hand, the secondary variables are also regulated within limits for all the studied values of  $\tau_d$ , as shown in Fig. 10a-d, Fig. 10e-h and Fig. 11e-h, for frequency,  $dc$ -voltage and  $ac$ -voltage, respectively.

A load step is applied in the  $ac$ -side between  $t = 30s$  and  $t = 60s$ . At  $t = 30s$ , loads  $Z_1$  and  $Z_3$  are increased to  $2.9 + j1.4kVA$  and  $2.8 + j1.4kVA$ , respectively. The initial power load condition is resumed at  $t = 60s$ , i.e.,  $Z_1 = 1.7 + j0.0kVA$  and  $Z_3 = 1.8 + j0.0kVA$ .

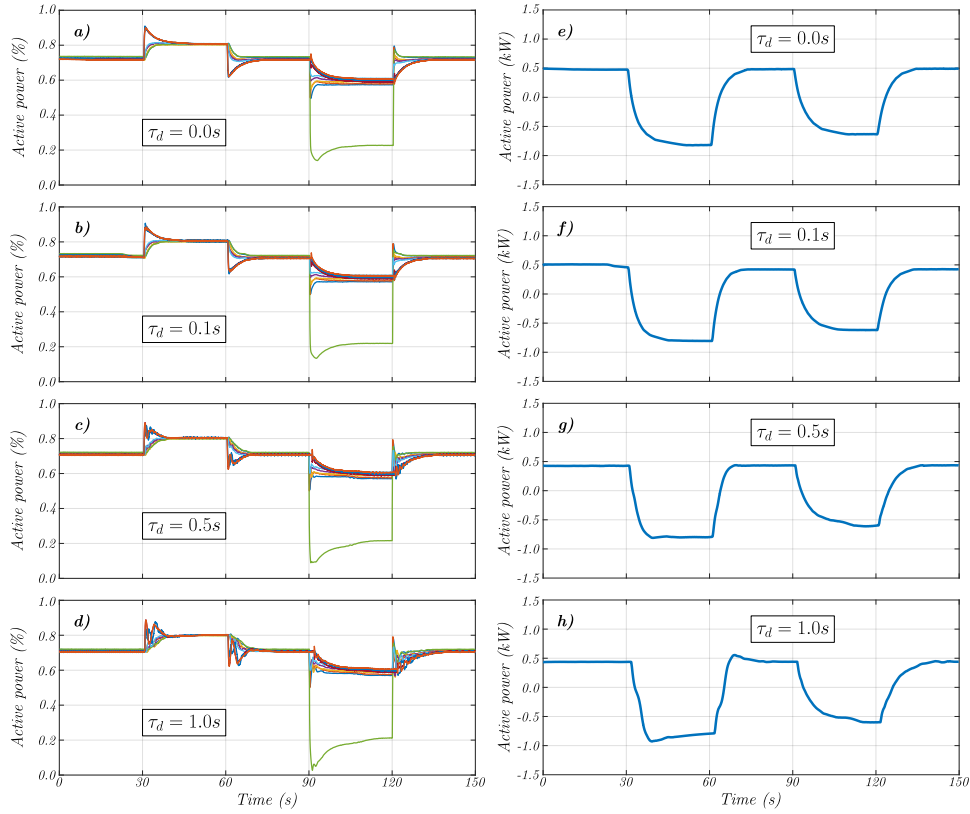


Fig. 9: Test #2: (a-d) Active power generated by  $ac$ -DGs ( $P_{ac-i}, i = 1, 2, 3$ ) and  $dc$ -DGs ( $P_{dc-j}, j = 1, \dots, 6$ ), in p.u. (e-h) Active power through the IC ( $P_{IC}$ ).

It can be seen that the control algorithm continues working correctly for all the studied values of  $\tau_d$ : the power consensus is achieved (see Fig. 9a-d and Fig. 11a-d for active and reactive power, respectively) and the secondary variables are maintained within limits (see Fig. 10a-d, Fig. 10e-h and Fig. 11e-h, for frequency,  $dc$ -voltage and  $ac$ -voltage, respectively). On the other hand, the power transferred by the IC is adjusted to help maintaining the power consensus among DGs (see Fig. 9e-h).

Between  $t = 90s$  and  $t = 120s$ , a load step is applied in the  $dc$ -side. At  $t = 90s$ , loads  $R_2$  and  $R_5$  on the  $dc$ -side are disconnected, and the base load condition is resumed at  $t = 120s$ , i.e.,  $R_2 = 2.05kW$  and  $R_5 = 2.05kW$ . As in the previous case, the control algorithm continues working correctly for all the studied values of  $\tau_d$ .

It is worth noting that, despite the control algorithm reaches the steady-state condition after applying the load steps at both sides of the hybrid  $ac/dc$ -microgrid, the transient response becomes more oscillatory as the delay increases. Moreover, the overshoot of the transient response also becomes larger for long delays. Therefore, the proposed control scheme is able to handle communication issues as communication delays; however, special attention has to be on the transient response in order to avoid surpassing the operational limits of the DGs.

## Conclusion

In this paper, the performance of the DSC strategy proposed in [10] in the presence of communication issues (communication loss and communication delay) was experimentally evaluated. It was shown that the control strategy is capable of restoring the secondary variables while maintaining an accurate power-sharing among the  $ac$ -DGs and  $dc$ -DGs when an agent is disconnected/reconnected from/to the communication network. Moreover, the control strategy can operate even when a long time-delay is applied to the entire communication network. The experimental tests demonstrate an excellent performance for the DSC strategy against common communication issues.

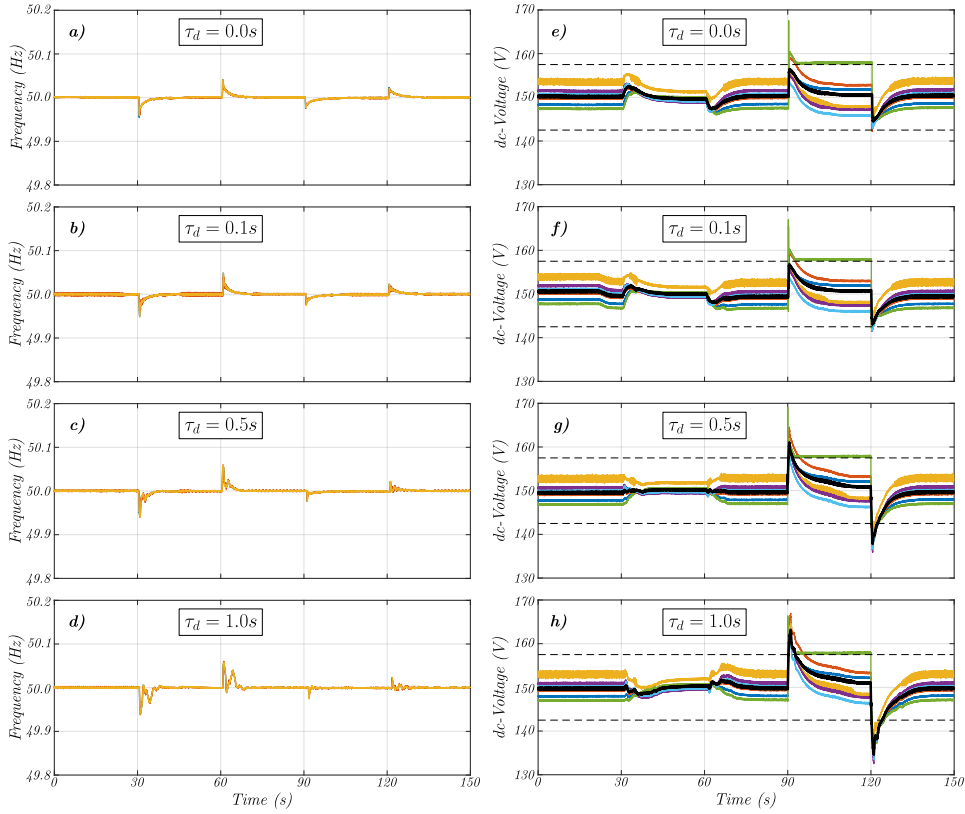


Fig. 10: Test #2: (a-d) Frequency of the voltages on the  $ac$ -DGs ( $f_i, i = 1, 2, 3$ ). (e-h) Voltages on the  $dc$ -DGs ( $V_j, j = 1, \dots, 6$ ).

## References

- [1] J. M. Guerrero, J. C. Vasquez, J. Matas, L. G. de Vicuna, and M. Castilla, "Hierarchical Control of Droop-Controlled AC and DC Microgrids: A General Approach Toward Standardization," *IEEE Transactions on Industrial Electronics*, vol. 58, no. 1, pp. 158–172, Jan 2011.
- [2] R. Majumder, B. Chaudhuri, A. Ghosh, R. Majumder, G. Ledwich, and F. Zare, "Improvement of Stability and Load Sharing in an Autonomous Microgrid Using Supplementary Droop Control Loop," *IEEE Trans. Power Syst.*, vol. 25, no. 2, pp. 796–808, May 2010.
- [3] M. A. Hossain, H. R. Pota, M. J. Hossain, and F. Blaabjerg, "Evolution of microgrids with converter-interfaced generations: Challenges and opportunities," *International Journal of Electrical Power and Energy Systems*, vol. 109, no. October 2018, pp. 160–186, 2019.
- [4] Y. Khayat, J. M. Guerrero, H. Bevrani, Q. Shafiee, R. Heydari, M. Naderi, T. Dragicevic, J. W. Simpson-Porco, F. Dörfler, M. Fathi, and F. Blaabjerg, "On the Secondary Control Architectures of AC Microgrids: An Overview," *IEEE Trans. Power Electron.*, vol. 35, no. 6, pp. 6482–6500, 2020.
- [5] T. Dragičević, X. Lu, J. C. Vasquez, and J. M. Guerrero, "DC Microgrids - Part II: A Review of Power Architectures, Applications, and Standardization Issues," *IEEE Trans. Power Electron.*, vol. 31, no. 5, pp. 3528–3549, 2016.
- [6] S. K. Sahoo, A. K. Sinha, and N. K. Kishore, "Control Techniques in AC, DC, and Hybrid AC-DC Microgrid: A Review," *IEEE Trans. Emerg. Sel. Topics Power Electron.*, vol. 6, no. 2, pp. 738–759, 2018.
- [7] E. Espina, J. Llanos, C. Burgos-Mellado, R. Cárdenas-Dobson, M. Martínez-Gómez, and D. Sáez, "Distributed control strategies for microgrids: An overview," *IEEE Access*, vol. 8, pp. 193 412–193 448, 2020.
- [8] J. W. Simpson-Porco, Q. Shafiee, F. Dörfler, J. C. Vasquez, J. M. Guerrero, and F. Bullo, "Secondary Frequency and Voltage Control of Islanded Microgrids via Distributed Averaging," *IEEE Trans. Ind. Electron.*, vol. 62, no. 11, pp. 7025–7038, Nov 2015.

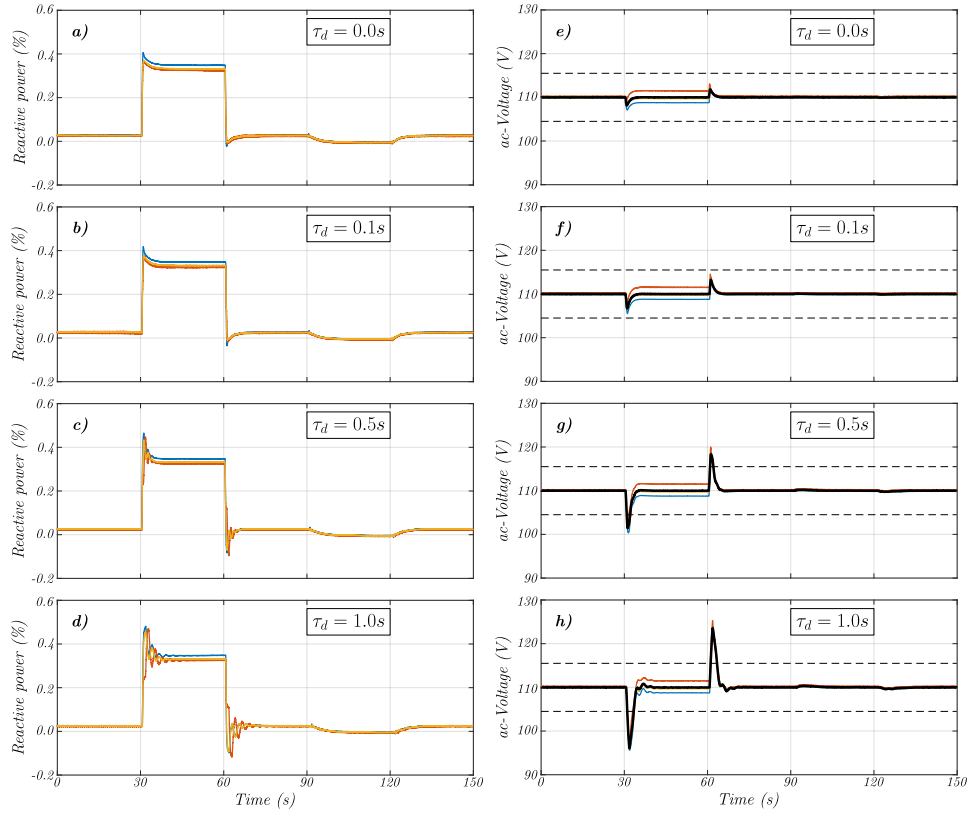


Fig. 11: Test #2: (a-d) Reactive power generated by  $ac$ -DGs ( $Q_i, i = 1, 2, 3$ ), in p.u. (e-h) Phase-to-neutral RMS voltages on the  $ac$ -DGs ( $V_i, i = 1, 2, 3$ ).

- [9] M. H. Cintuglu, T. Youssef, and O. A. Mohammed, "Development and Application of a Real-Time Testbed for Multiagent System Interoperability: A Case Study on Hierarchical Microgrid Control," *IEEE Transactions on Smart Grid*, vol. 9, no. 3, pp. 1759–1768, may 2018.
- [10] E. Espina, R. Cárdenas-Dobson, J. W. Simpson-Porco, D. Sáez, and M. Kazerani, "A consensus-based secondary control strategy for hybrid ac/dc microgrids with experimental validation," *IEEE Transactions on Power Electronics*, pp. 1–1, 2020.
- [11] F. Nejabatkhah, Y. W. Li, and H. Tian, "Power quality control of smart hybrid AC/DC microgrids: An overview," *IEEE Access*, vol. 7, pp. 52 295–52 318, 2019.
- [12] A. A. Jabbar, A. Y. Elrayyah, M. Z. Wanik, A. P. Sanfilippo, and N. K. Singh, "Development of Hybrid AC/DC Laboratory-scale Smart Microgrid Testbed with Control Monitoring System Implementation in LabVIEW," in *IEEE Grand Int. Conf. Expo. Asia (GTD Asia)*, 2019, pp. 889–894.
- [13] C. Jin, P. Wang, J. Xiao, Y. Tang, and F. H. Choo, "Implementation of Hierarchical Control in DC Microgrids," *IEEE Trans. Ind. Electron.*, vol. 61, no. 8, pp. 4032–4042, Aug 2014.
- [14] W. Yao, M. Chen, J. Matas, J. M. Guerrero, and Z. M. Qian, "Design and Analysis of the Droop Control Method for Parallel Inverters Considering the Impact of the Complex Impedance on the Power Sharing," *IEEE Trans. Ind. Electron.*, vol. 58, no. 2, pp. 576–588, Feb 2011.
- [15] J. S. Gómez, D. Sáez, J. W. Simpson-Porco, and R. Cárdenas, "Distributed predictive control for frequency and voltage regulation in microgrids," *IEEE Trans. Smart Grid*, vol. 11, no. 2, pp. 1319–1329, March 2020.
- [16] I. Serban, S. Cspedes, C. Marinescu, C. A. Azurdia-Meza, J. S. Gmez, and D. S. Hueichapan, "Communication requirements in microgrids: A practical survey," *IEEE Access*, vol. 8, pp. 47 694–47 712, 2020.
- [17] A. Bidram, V. Nasirian, A. Davoudi, and F. Lewis, *Cooperative Synchronization in Distributed Microgrid Control*, 01 2017.
- [18] E. Espina, C. Burgos-Mellado, J. S. Gomez, J. Llanos, E. Rute, A. Navas F., M. Martínez-Gómez, R. Cárdenas, and D. Sáez, "Experimental hybrid ac/dc-microgrid prototype for laboratory research," in *2020 22nd European Conference on Power Electronics and Applications (EPE'20 ECCE Europe)*, 2020, pp. 1–9.